SURFACE FLUID REGISTRATION OF CONFORMAL REPRESENTATION: APPLICATION TO DETECT DISEASE BURDEN AND GENETIC INFLUENCE ON HIPPOCAMPUS

Jie Shi MS[1], Paul M. Thompson PhD[2], Boris Gutman BS[2], Yalin Wang PhD[1], For the Alzheimer's Disease Neuroimaging Initiative[*]

[1]School of Computing, Informatics, and Decision Systems Engineering, Arizona State University, Tempe, AZ, USA
[2]Laboratory of Neuro Imaging, UCLA Dept. of Neurology, UCLA School of Medicine, Los Angeles, CA, USA

Published in *NeuroImage*

Please address correspondence to:
Dr. Yalin Wang
School of Computing, Informatics, and Decision Systems Engineering
Arizona State University
P.O. Box 878809
Tempe, AZ 85287 USA
Phone: (480) 965-6871
Fax: (480) 965-2751
E-mail: ylwang@asu.edu

***Acknowledgments and Author Contributions:** Data used in preparation of this article were obtained from the Alzheimer's Disease Neuroimaging Initiative (ADNI) database (adni.loni.ucla.edu). As such, the investigators within the ADNI contributed to the design and implementation of ADNI and/or provided data but did not participate in analysis or writing of this report. A complete listing of ADNI investigators can be found at: http://adni.loni.ucla.edu/wp-content/uploads/how_to_apply/ADNI_Acknowledgement_List.pdf. Additional support was provided by the National Institute on Aging (AG016570 to PMT), the National Library of Medicine, the National Institute for Biomedical Imaging and Bioengineering, and the National Center for Research Resources (LM05639, EB01651, RR019771 to PMT).

ABSTRACT

In this paper, we develop a new automated surface registration system based on surface conformal parameterization by holomorphic 1-forms, inverse consistent surface fluid registration, and multivariate tensor-based morphometry (mTBM). First, we conformally map a surface onto a planar rectangle space with holomorphic 1-forms. Second, we compute surface conformal representation by combining its local conformal factor and mean curvature and linearly scale the dynamic range of the conformal representation to form the feature image of the surface. Third, we align the feature image with a chosen template image via the fluid image registration algorithm, which has been extended into the curvilinear coordinates to adjust for the distortion introduced by surface parameterization. The inverse consistent image registration algorithm is also incorporated in the system to jointly estimate the forward and inverse transformations between the study and template images. This alignment induces a corresponding deformation on the surface. We tested the system on Alzheimer's Disease Neuroimaging Initiative (ADNI) baseline dataset to study AD symptoms on hippocampus. In our system, by modeling a hippocampus as a 3D parametric surface, we nonlinearly registered each surface with a selected template surface. Then we used mTBM to analyze the morphometry difference between diagnostic groups. Experimental results show that the new system has better performance than two publically available subcortical surface registration tools: FIRST and SPHARM. We also analyzed the genetic influence of the Apolipoprotein E $\epsilon 4$ allele (ApoE4), which is considered as the most prevalent risk factor for AD. Our work successfully detected statistically significant difference between ApoE4 carriers and non-carriers in both patients of mild cognitive impairment (MCI) and healthy control subjects. The results show evidence that the ApoE genotype may be associated with accelerated brain atrophy so that our work provides a new MRI analysis tool that may help presymptomatic AD research.

Key Words: nonlinear image registration, surface conformal parameterization, conformal representation, surface fluid registration, tensor-based morphometry, presymptomatic AD

1. INTRODUCTION

Most brain MRI scanning protocols have been designed to acquire volumetric data on the anatomy of a subject. Various non-linear brain volume-based registration methods (Christensen et al., 1996; Shen and Davatzikos, 2002; Yanovsky et al., 2009) have been developed for brain volume image analysis. However, when registering structural MR images, the volume-based methods have much more difficulty with the highly convoluted cortical surfaces due to the complexity and variability of the sulci and gyri. Early research (Thompson and Toga, 1996; Fischl et al., 1999; Van Essen et al., 2001; Thompson et al., 2004b) has demonstrated that surface-based brain mapping may offer advantages over volume-based brain mapping as a method to study the structural features of the brain, such as cortical gray matter thickness, as well as the complexity and change patterns in the brain due to disease or developmental processes. To register brain surfaces, a common approach is to compute dense

correspondence vector fields that match one surface with another. Often, higher order correspondences must be enforced between specific anatomical points, curved landmarks, or subregions lying within two surfaces. This is often achieved by first mapping each of the 3D surfaces to a canonical parameter space such as a sphere (Bakircioglu et al., 1999; Fischl et al., 1999; Yeo et al., 2010) or a planar domain (Thompson and Toga, 2002; Thompson et al., 2004b; Leow et al., 2005b). A flow, computed in the parameter space of the two surfaces, induces a correspondence field in 3D (Davatzikos, 1996; Thompson et al., 2000). This flow can be constrained using anatomic landmark points or curves (Pantazis et al., 2010; Zhong and Qiu, 2010; Auzias et al., 2011), by subregions of interest (Qiu and Miller, 2008), by constraining the mapping of surface regions represented implicitly using level sets (Leow et al., 2005b), or by using currents to represent anatomical variation (Vaillant and Glaunes, 2005; Vaillant et al., 2007; Durrleman et al., 2008). Feature correspondence between two surfaces can be optimized by using the ℓ_2-norm to measure differences in curvature profiles or convexity (Fischl et al., 1999) or by using mutual information to align scalar fields of various differential geometric parameters defined on the surface (Wang et al., 2005b). Artificial neural networks may also be used to rule out or favor certain types of feature matches (Pitiot et al., 2003). Finally, correspondences may be determined by using a minimum description length (MDL) principle, based on the compactness of the covariance of the resulting shape model (Davies et al., 2002; Thodberg, 2003). A key direction in surface registration research has been the computation of a diffeomorphic surface map that matches automatically identified surface features.

MRI-based measures of atrophy in several structural measures, including whole-brain (Fox et al., 1999; Chen et al., 2007; Stonnington et al., 2010), entorhinal cortex (Cardenas et al., 2011), hippocampus (Jack et al., 2003; Thompson et al., 2004a; Wang et al., 2006; den Heijer et al., 2010; Wolz et al., 2010), and temporal lobe volumes (Hua et al., 2011), as well as ventricular enlargement (Jack et al., 2003; Thompson et al., 2004a), correlate closely with changes in cognitive performance, supporting their validity as markers of disease progression (Apostolova et al., 2010b; Costafreda et al., 2011). Of all the MRI markers of Alzheimer's disease (AD), hippocampal atrophy assessed on high-resolution T1-weighted MRI is the best established and validated. One of the key research topics for clinical assessment in diagnosis and monitoring of progression of patients with suspected Alzheimer dementia is to establish and validate efficient biomarkers based on subcortical structures including hippocampus. Although most subcortical structure analysis work used volume as the atrophy measurement (Jack et al., 2003; Jack et al., 2004; Ridha et al., 2008; Holland et al., 2009; den Heijer et al., 2010; Dewey et al., 2010; Wolz et al., 2010), recent researches (Thompson et al., 2004a; Styner et al., 2005; Wang et al., 2006; Ferrarini et al., 2008; Chou et al., 2009; Morra et al., 2009b; Apostolova et al., 2010b; Apostolova et al., 2010c; Madsen et al., 2010; Qiu et al., 2010; Costafreda et al., 2011) have demonstrated that surface-based subcortical structure analysis may offer advantages over volume measure. For example, the surface-based methods have studied patterns of hippocampal subfield atrophy and detailed point-wise correlation between atrophy and cognitive functions/biological markers. There are several methods that match surfaces of subcortical structures using parametric surfaces, such as contour

anatomical changes. Chung et al. (2008) showed that the single value of the determinant of Jacobian can reliably detect surface morphometry due to autism. In our system, we use multivariate statistics based on surface deformation tensors to study brain surface morphometry as proposed in (Leporé et al., 2008; Wang et al., 2008). The multivariate tensor-based morphometry (mTBM) computes statistics from the Riemannian metric tensors that retain the full information in the deformation tensor fields, thus may be more powerful in detecting surface difference than many other statistics (Wang et al., 2009a; Wang et al., 2010b; Wang et al., 2011b; Wang et al., 2012b). Our hypothesis is that, together with mTBM as the surface statistics, our surface fluid registration method may help boost statistical power to detect disease burden and genetic influence on hippocampal morphometry compared with some existing researches in the literature. Here we set out to validate our algorithm in the Alzheimer's Disease Neuroimaging Initiative (ADNI) baseline dataset.

Fig. 1 summarizes the overall step sequence in our system. The brain MR image data was from ADNI baseline dataset. The hippocampal regions and surfaces were segmented and constructed automatically. We then computed hippocampal surface conformal parameterization with holomorphic 1-forms and obtained their feature images consisting of conformal factor and mean curvature. With the inverse consistent surface fluid registration method, we enforced symmetric displacements in both surfaces ($\boldsymbol{h}(\boldsymbol{x})$ denotes the forward mapping and $\boldsymbol{g}(\boldsymbol{x})$ denotes the inverse mapping, where $\boldsymbol{g}(\boldsymbol{x}) = \boldsymbol{h}^{-1}(\boldsymbol{x})$). Multivariate statistics were computed to study differences between diagnostically different groups and the genetic influence on Alzheimer's disease.

2. SUBJECTS AND METHODS

2.1. Subjects

Data used in the preparation of this article were obtained from the Alzheimer's Disease Neuroimaging Initiative (ADNI) database (adni.loni.ucla.edu). The ADNI was launched in 2003 by the National Institute on Aging (NIA), the National Institute of Biomedical Imaging and Bioengineering (NIBIB), the Food and Drug Administration (FDA), private pharmaceutical companies and non-profit organizations, as a $60 million, 5-year public-private partnership. The primary goal of ADNI has been to test whether serial magnetic resonance imaging (MRI), positron emission tomography (PET), other biological markers, and clinical and neuropsychological assessment can be combined to measure the progression of mild cognitive impairment (MCI) and early Alzheimer's disease (AD). Determination of sensitive and specific markers of very early AD progression is intended to aid researchers and clinicians to develop new treatments and monitor their effectiveness, as well as lessen the time and cost of clinical trials.

The Principal Investigator of this initiative is Michael W. Weiner, MD, VA Medical Center and University of California – San Francisco. ADNI is the result of efforts of many co-investigators from a broad range of academic institutions and private corporations, and subjects have been recruited from over 50 sites across the U.S. and

2003; Sun et al., 2007; Sun et al., 2008; Li et al., 2009) have also drawn more and more interests. In this paper, we applied a two-step mesh smoothing method to all the surfaces. The smoothing process consists of mesh simplification using "progressive meshes" (Hoppe, 1996) and mesh refinement by Loop subdivision surface (Loop, 1987). All the meshes were smoothed by 5 iterations of mesh simplification using "progressive meshes" and Loop subdivision. In order to smooth the surfaces while preserve surface features, we gradually increased the face numbers of the surfaces in each iteration. As a result, we obtained relatively smooth but accurate surfaces that are suitable for computing derivative maps. **Fig. 2** illustrates the histograms of the Hausdorff distances between the smoothed meshes and the original meshes for both the left and right hippocampi. We can see from the figure that the majority of the absolute distances fall into the range [0.9, 1.1] with the unit as millimeter. Given the volumes of hippocampus lie between 3000 and 4000 mm^3 (Hasboun et al., 1996; Hickie et al., 2005; Ystad et al., 2009; Carmichael, 2011), our smoothed meshes can be regarded as accurate approximations of the original surfaces. We applied this method in our prior subcortical surface analysis work (Wang et al., 2010b; Wang et al., 2011b). From our experience, a continuous subdivision and mesh simplification process will generally eliminate the obtuse angles and improve the mesh quality. Later all the smoothed meshes were normalized into a standard space using affine transformation with a 9-parameter (3 parameters for translation, 3 parameters for rotation, and 3 parameters for scaling) matrix that was computed by FIRST. In our study, 1 subject from each group (AD, MCI, and control) failed the FIRST segmentation step probably due to the original images' resolution or contrast issues. We also manually checked all the constructed and smoothed meshes and excluded 5 AD, 5 MCI, and 3 control subjects due to wrong topologies. As a result, the baseline MR hippocampus image data of 194 AD (age: 76.1$\pm$7.6 years), 402 MCI (age: 75.0$\pm$7.3 years), and 228 controls (age: 76.0$\pm$5.0 years) were studied using the new system within the scope of this paper.

2.3. Surface Conformal Parameterization with Holomorphic 1-Forms

Let S be a surface in $\mathbb{R}^3$ with an atlas $\{(U_\alpha, z_\alpha)\}$, where (U_α, z_α) is a coordinate chart defined on S. The atlas thus is a set of consistent charts with smooth transition functions between overlapping charts. Here $z_\alpha: U_\alpha \to \mathbb{C}$ maps an open set $U_\alpha \subset S$ to a complex plane $\mathbb{C}$. If on any chart (U_α, z_α) in the atlas, the Riemannian metric or the first fundamental form can be formulated as $ds^2 = \lambda(z_\alpha)^2 dz_\alpha d\bar{z}_\alpha$, and the transition maps $z_\beta \circ z_\alpha^{-1}: z_\alpha(U_\alpha \cap U_\beta) \to z_\beta(U_\alpha \cap U_\beta)$ are holomorphic, the atlas could be called conformal. Given a conformal atlas, a chart is compatible with the atlas if adding this chart still generates a conformal atlas. A conformal structure is obtained by adding all possible compatible charts to a conformal atlas. A Riemann surface is a surface with a conformal structure. All metric oriented surfaces are Riemann surfaces. One coordinate chart in the conformal structure introduces a conformal parameterization between a surface patch and the image plane. The conformal parameterization is angle-preserving and intrinsic to the surface geometry (Do Carmo, 1976; Guggenheimer, 1977).

For a Riemann surface S with genus g > 0, its conformal structure can always be represented in terms of a holomorphic 1-form basis, which is a set of 2g functions $\tau_i: K_1 \to \mathbb{C}, i = 1, \dots, 2g$ (Wang et al., 2007). Here, K_1 represents the simplicial 1-complex*. Any holomorphic 1-form τ is a linear combination of these functions. This finite-dimensional linear space generates all possible conformal parameterizations of surface S and the quality of a global conformal parameterization is fundamentally determined by the choice of the holomorphic 1-form (Wang et al., 2007; Wang et al., 2011b). By considering the holomorphic 1-form as an $\mathbb{R}^2$ function, the conformal parameterization $\phi: S \to \mathbb{R}^2$ at point p can be computed by integrating the holomorphic 1-form:

$$\phi(p) = \int_\gamma \tau. \tag{1}$$

where γ is an arbitrary path joining p to a fixed point p_0 on the surface. The details of our holomorphic 1-form based conformal parameterization algorithms were reported in our prior work (Wang et al., 2007; Wang et al., 2011b). **Fig. 3** (a) illustrates a pair of hippocampal surfaces and their conformal parameterizations to a rectangular domain.

2.4. Surface Conformal Representation

It has been known that surface registration requires defining a lot of landmarks in order to align corresponding functional regions. Labeling features could be accurate but time-consuming. Here we show that surface conformal parameterization could represent surface geometric features, thus avoiding the manual definition of landmarks.

For a general surface and its conformal parameterization $\phi: S \to \mathbb{R}^2$, the conformal factor at a point p can be determined by the formula:

$$\lambda(p) = \frac{\text{Area}(B_\epsilon(p))}{\text{Area}(\phi(B_\epsilon(p)))}. \tag{2}$$

where $B_\epsilon(p)$ is an open ball around p with a radius ϵ. The conformal factor λ encodes a lot of geometric information about the surface and can be used to compute curvatures and geodesic. In our system, we compute the surface mean curvatures only from the derivatives of the conformal factors as proposed in Lui et al. (2008a), instead of the three coordinate functions and the normal, which are generally more sensitive to digitization errors. Mathematically, the mean curvature is defined as:

$$H = \frac{1}{2\lambda}\text{sign}(\phi)|\Delta\phi| \tag{3}$$

* In mathematics, a simplicial complex is a topological space that is constructed by gluing together points, line segments, triangles, and their n-dimensional counterparts. A simplicial k-complex K_k is a slimplicial complex where the largest dimension of any component in K_k equals to k. In our settings, a simplicial 1-complex is an edge.

where $\text{sign}(\phi) = \frac{<\Delta\phi, \vec{N}>}{|\Delta\phi|}$. Using this formulation of H, we need to use the surface normal $\vec{N}$ only when computing $\text{sign}(\phi)$, which takes the value 1 or -1. Thus, the surface normal does not need to be accurately estimated and still we can get more accurate mean curvatures. Using the Gauss and Codazzi equations, one can prove that the conformal factor and mean curvature uniquely determine a closed surface in $\mathbb{R}^3$, up to a rigid motion (Gu et al., 2004b). We call them the conformal representation of the surface. **Fig. 3** (b) shows the computed conformal factor (left) and mean curvature (right) on a hippocampal surface with color indices according to the values. Since conformal factor and mean curvature encode both surface intrinsic structure and 3D embedding information, they are complete surface features to be used for solving surface registration problems (Gu and Vemuri, 2004; Wang et al., 2005a).

2.5. Inverse Consistent Surface Fluid Registration

After computing surface geometric features, we align surfaces in the parameter domain with a fluid registration technique to maintain smooth, one-to-one topology (Christensen et al., 1996). Using conformal mapping, we essentially convert the surface registration problem to an image registration problem. In our prior work (Wang et al., 2005a), we proposed an automated surface fluid registration method combining conformal mapping and image fluid registration (D'Agostino et al., 2003) with mutual information (Kim et al., 1997; Meyer et al., 1997; West et al., 1997; Rueckert et al., 1999; Hermosillo, 2002) as the driving force of the viscous fluid. In Wang et al. (2005a), the mutual information between two surface feature images, i.e., the conformal representations of the two surfaces that need to be registered, was maximized by the viscous fluid flow as in D'Agostino et al. (2003). On $\mathbb{R}^2$, fluid flow is governed by the Navier-Stokes equation. For compressible fluid flow, we have

$$\mu\Delta\boldsymbol{v}(\boldsymbol{x}) + (\mu + \tau)\nabla\big(\nabla \cdot \boldsymbol{v}(\boldsymbol{x})\big) = \boldsymbol{f}\big(\boldsymbol{x}, \boldsymbol{u}(\boldsymbol{x})\big). \tag{4}$$

Here $\boldsymbol{v}(\boldsymbol{x})$ is the deformation velocity, μ and τ are the viscosity constants. $\boldsymbol{f}(\boldsymbol{x}, \boldsymbol{u}(\boldsymbol{x}))$ is the force field that is used to drive the fluid flow, which was defined as the mutual information in Wang et al. (2005a).

To simulate fluid flow on Riemann surfaces, we need to extend **Eq. 4** into surface space by the manifold version of Laplacian and divergence (Aris, 1989; Stam, 2003; Lui et al., 2005). By covariant derivatives, the Navier-Stokes equation for Riemann surface can be defined as:

$$\frac{\mu}{\lambda}\Delta\boldsymbol{v} + \frac{\mu+\tau}{\lambda}\nabla(\nabla \cdot \boldsymbol{v}) = \boldsymbol{f}. \tag{5}$$

where λ is the conformal factor as introduced in Sec. 2.4. Please refer the appendix A for the derivation of **Eq. 5**. It is well known that area distortion is an inevitable problem of conformal parameterization. However, considering the definition of conformal factor λ as **Eq. 2**, we can see that conformal factor is a smooth function which describes the stretching effect of conformal parameterization (Lui et al., 2008b). In **Eq. 5**, by factoring out the conformal factor λ, the flow induced in the parameter domain is adjusted for the area distortion introduced by

between the tangent spaces, $d\phi: TM(p) \rightarrow TM(\phi(p))$, induced by the map ϕ. In the local parameter domain, the derivative map is the Jacobian of ϕ:

$$d\phi = \begin{bmatrix} \frac{\partial \phi_1}{\partial u_1} & \frac{\partial \phi_1}{\partial v_1} \\ \frac{\partial \phi_2}{\partial u_1} & \frac{\partial \phi_2}{\partial v_1} \end{bmatrix}$$

Let the position vector of S_1 be $\mathrm{r}(u_1, v_1)$. Denote the tangent vector fields as $\frac{\partial}{\partial u_1} = \frac{\partial \mathrm{r}}{\partial u_1}$, $\frac{\partial}{\partial v_1} = \frac{\partial \mathrm{r}}{\partial v_1}$. Because (u_1, v_1) are isothermal coordinates, $\frac{\partial}{\partial u_1}$ and $\frac{\partial}{\partial v_1}$ only differ by a rotation of $\pi/2$. Therefore, we can construct an orthonormal frame on the tangent plane of S_1 as $\{e^{-\lambda_1}\frac{\partial}{\partial u_1}, e^{-\lambda_1}\frac{\partial}{\partial v_1}\}$.

Similarly, we can construct an orthonormal frame on S_2 for its isothermal coordinates. Since any two surfaces are locally conformal (Hsiung, 1997), we can have an orthonormal frame on S_2 as $\{e^{-\lambda_2}\frac{\partial}{\partial u_1}, e^{-\lambda_2}\frac{\partial}{\partial v_1}\}$. The derivative map under the orthonormal frames is represented as

$$d\phi = e^{\lambda_2 - \lambda_1}\begin{bmatrix} \frac{\partial \phi_1}{\partial u_1} & \frac{\partial \phi_1}{\partial v_1} \\ \frac{\partial \phi_2}{\partial u_1} & \frac{\partial \phi_2}{\partial v_1} \end{bmatrix}$$

In practice, smooth surfaces are approximated by triangle meshes. In the triangle mesh surface, the derivative map $d\phi$ is approximated by the linear map from one face $[v_1, v_2, v_3]$ to another $[w_1, w_2, w_3]$. First, the surfaces $[v_1, v_2, v_3]$ and $[w_1, w_2, w_3]$ are isometrically embedded onto the plane $\mathbb{R}^2$ (i.e., $\lambda_1 = \lambda_2 = 0$ in the above equation), the planar coordinates of the vertices v_i, w_i are denoted by the same symbol v_i, w_i. Then the Jacobian matrix for the derivative map $d\phi$ can be explicitly computed as (Wang et al., 2009a)

$$J = d\phi = [w_3 - w_1, w_2 - w_1][v_3 - v_1, v_2 - v_1]^{-1}. \quad (10)$$

The deformation tensor can be defined as $S = (J^T J)^{\frac{1}{2}}$ (Chung et al., 2001; Hua et al., 2011). Instead of analyzing shape change based on the eigenvalues of the deformation tensor, a new family of metrics, the "Log-Euclidean metrics" (Arsigny et al., 2006) is considered in the multivariate tensor-based morphometry (mTBM). In this framework, Riemannian computations can be converted into Euclidean ones once tensors have been transformed into their matrix logarithms (Arsigny et al., 2006). This conversion makes computations on tensors easier to perform, as they are chosen such that the transformed values form a vector space, and statistical parameters can then be computed easily using the standard formulae for Euclidean spaces (Leporé et al., 2008; Wang et al., 2008).

To compute group differences with mTBM, we then apply Hotelling's T^2 test (Hotelling, 1931; Cao and Worsley, 1999; Thirion et al., 2000; Kim et al., 2012) on sets of values in the log-Euclidean space of the deformation

(5). Group difference between ApoE4 carriers and non-carriers in AD patients.

Fig. 8 shows our experimental results when we used mTBM as the surface statistics. In our study, we used all available samples from ADNI baseline dataset. Among the 824 subjects, 725 subjects have been diagnosed as ApoE4 carriers or non-carriers (366 non-carriers vs. 359 carriers), 558 of which are MCI or controls (310 non-carriers vs. 248 carriers). **Fig. 8** (a) and (b) show the significance maps for the two experiments. **Fig. 8** (b) illustrated the results on ApoE4 effects on both healthy control and MCI groups. Our results suggested more significant areas were detected on the left side. The permutation test results showed our method detected significant difference between ApoE4 carriers and ApoE4 non-carriers in healthy subjects and patients with MCI (p=0.0014). A few studies to date have investigated ApoE4 effect on the hippocampal atrophy at the subregional level (Morra et al., 2009a; Mueller and Weiner, 2009; Pievani et al., 2011). Among them one study failed to detect an effect (Morra et al., 2009a) and others (Mueller and Weiner, 2009; Pievani et al., 2011) detected effects. However, Mueller and Weiner (2009) investigated a rather small ApoE4 sample (n=5 patients) and Pievani et al. (2011) used the manually traced hippocampal contours to segment the hippocampal shape in a small patient data set (n=28 patients). Our work is the first study, to our knowledge, which found ApoE4 effect on subregional hippocampal atrophy in healthy subjects and MCI patients in the ADNI dataset. Our method used an automatic image segmentation method to segment hippocampus so our method may have the high throughput advantage. Our results, more significant areas on the left side than on the right side, may also agree with the prior discovery (Pievani et al., 2011) where the effect of ApoE4 mapping was statistically significant on left hippocampus whereas statistically insignificant on the right hippocampus.

Among the 228 healthy controls, 150 subjects are diagnosed as ApoE4 non-carriers; among the 194 AD patients, 56 subjects are diagnosed as ApoE4 non-carriers and 111 subjects ApoE4 carriers. We conducted group difference experiments (3)-(5) among these three groups. **Fig. 8** (c)-(e) show the significance maps of the three experiments. With mTBM, our system detected significant atrophy areas in group difference experiments (1)-(4). In the last experiment (5), our system detected consistent significant areas on the left hippocampus and more significant areas on the right hippocampus than (Pievani et al., 2011), whereas the significant p-value is 0.0581, which is statistically insignificant.

For comparison purpose, we also tested with the other two surface registration methods as in Sec. 3.4. As we mentioned above, we excluded the 4 AD and 6 MCI subjects that failed in SPHARM from our studying dataset used in the surface fluid and FIRST experiments. As a result, among the 814 subjects, 715 subjects have been diagnosed as ApoE4 carriers or non-carriers (360 non-carriers vs. 355 carriers), 552 of which are MCI or controls (306 non-carriers vs. 246 carriers); among the 228 healthy controls, 150 subjects are diagnosed as ApoE4 non-carriers; among the 190 AD patients, 54 subjects are diagnosed as ApoE4 non-carriers and 109 subjects ApoE4 carriers. **Fig. 9** shows the significance p-maps of all five experiments with FIRST as the surface registration

Fig. 5. In our experiments, we applied the inverse consistent surface fluid registration on both directions to register surface 1 to surface 2 (the first row in **Fig. 13**) and surface 2 to surface 1 (the second row in **Fig. 13**). We tried to perform the registrations with or without the parameterization compensation terms. We also visualized the pull-back metrics by drawing those equal-spaced black strips defined on the target surfaces back to the source surfaces based on the registration. It is obvious that the registration results with the area distortion correction ((c) and (d)) have more uniform strips than those without the area distortion correction ((e) and (f)). Similar to prior work (Stam, 2003; Thompson et al., 2004b; Lui et al., 2005; Wang et al., 2007), this simple example may help justify our formulation and demonstrate its efficacy to produce a good surface correspondence.

ϵ-Isometric parameterization vs conformal parameterization Mathematically speaking, an isometric mapping between two surfaces requires that the first fundamental forms to be equivalent throughout the surfaces whereas a conformal mapping only requires the first fundamental forms to be different by a scalar. As a result, the conditions for conformal mapping are relatively loose. Similar to the cartography problems, it is impossible to compute a mapping from the hippocampal surface to a Euclidean plane that preserves all the geodesic distances. This is a consequence of the theorema egregium (Do Carmo, 1976): because the Gaussian curvature of the hippocampal surface is nonzero on most of surface areas, whereas the plane has zero curvature, these two surfaces cannot be isometric. In the computer graphics and computer vision fields, there were numerous methods proposed to compute the ϵ-isometric parameterization, i.e. an approximation of isometric mapping, e.g. some methods (Schwartz et al., 1989; Bronstein et al., 2006) apply a multidimensional scaling method (Torgerson, 1952; Shepard, 1962; Kruskal, 1964b; a) to compute the near-isometry mapping to the plane for retinotopic mapping and 3D face recognition study.

On the other hand, conformal parameterization was adopted in various imaging and graphics applications to study surface registration (Lipman and Funkhouser, 2009; Boyer et al., 2011; Wang et al., 2012b). Because of the uniformization theorem, conformal mappings to certain domains exist on every simply connected Riemann surface. The discrete conformal mapping has a rigorous theoretic definition and can be computed accurately. In our study, there exists a conformal mapping from a hippocampal surface with two introduced cuts to the Euclidean plane. Our prior work (Wang et al., 2007) introduced a holomorphic 1-form based method to compute such a conformal mapping. Although there are area distortions on a conformal mapping, considering the definition of conformal factor λ as **Eq. 2**, we can see that conformal factor is a smooth function which describes the stretching effect of conformal parameterization. With the conformal factor as the compensation term, the major novelty of the current work is to introduce the Navier-Stokes equation for Riemann surface by the covariant derivatives. Specifically, in **Eq. 5**, by dividing the conformal factor λ, the flow induced in the parameter domain is adjusted for the area distortion introduced by the conformal parameterization and one may achieve a coordinate invariant PDE solving formulation. The proposed formulation is simpler than the prior work (Thompson and

Toga, 2002; Thompson et al., 2004b) and may offer a numerically stable and efficient method for surface registration problem.

Comparison with isometry-based surface registration methods. Many existed isometry-based algorithms have focused on mappings of surfaces to their flattened ones on the Euclidean plane (Timsari and Leahy, 2000; Sander et al., 2001; Zigelman et al., 2002; Balasubramanian et al., 2010). Some research also tried to enforce either distance preserving or near-isometry in the surface registration work (Schreiner et al., 2004; Eckstein et al., 2007; Cho et al., 2011). Among them, Cho et al. (2011) proposed a multi-resolution distortion-minimizing mapping scheme to compute surface correspondence between subcortical surfaces. The same research problem that we are trying to address may justify the effort to briefly compare our work with their work.

In (Cho et al., 2011), although they do not map a hippocampal surface to the Euclidean plane, they employ an area-preserving approximation spherical parameterization method (Shen and Makedon, 2006) to establish an initial surface alignment and, for each iteration, generalize the mapping from the low resolution meshes to high resolution meshes. In the registration step, they formulate the matching problem as an energy minimization problem that is defined on a high-dimensional Riemannian manifold and penalizes the deviation from isometric mapping and triangle flippings. The surface deformation is constrained to move along the source surfaces. Our work formulates the surface registration as an image flow problem so that we convert a 3D registration problem to a 2D one via the conformal parameterization. Because of the nature of 2D image registration, our work is more intuitive and easier to be visualized. Due to the differential covariants, our work compares vector fields and deforms surfaces on their tangent planes and also deforms surfaces on surfaces themselves (both source and target surfaces). Furthermore, the inverse consistent registration framework helps maintain a symmetric correspondence and does not depend on the order we use to compare surfaces. Overall, these two papers take two different approaches, i.e. one projects the matching problem to a high-dimensional Riemannian manifold and pursues an approximated isometry deformation while the other converts the problem to the 2D image plane and solves it with some stable 2D image registration schemes. Although a quantitative comparison may be of interest for future work, two algorithms are comparable and complementary to each other. We expect one method may outperform the other in some contexts but not others, or in some diseases but not others, depending on the type of surfaces to be registered.

Benefits of conformal parameterization. For surface morphometry study, one traditional way to do this is to set up parametric grids on surfaces, which are registered across subjects, and then use differential geometry to come up with useful descriptors of surface features of interest, or to summarize the geometry as a whole. Conformal maps help to induce particularly well-organized grids on surfaces. This simplifies a number of downstream computations of registration and surface metrics. The major benefits of conformal parameterization in our work include: (1) a good initialization alignment. For two similar shapes, their conformal structures are also similar. As

Does the cutting affect the statistics? To achieve an accurate registration between surfaces, we cut open two landmark curves and convert the landmark matching problem as an explicit boundary matching problem. We have adopted this approach in our prior work on brain cortical surface registration (Wang et al., 2012b) and subcortical surface registration (Wang et al., 2011b). The topology cuts do not change the overall surface geometry because the two sides of the cuts are still in the identical positions. So the cuts do not affect the surface registration and the following shape analysis work. Also since we have the conformal factor as the compensation term for the area distortion in the fluid registration framework, theoretically these cuts should not affect the statistical results on the neighboring regions. As shown in **Fig. 14**, the enlarged figures highlight the positions of the landmark curves and the insignificant regions on the p-map. We can see that the statistically insignificant area does not align exactly with the cutting positions. However, to achieve an accurate surface registration and morphometry analysis, the cut positions need to be consistent across subjects. Besides the automatic moment-based landmark curve identification method discussed in Sec. 3.2, we also applied a quality control step by manually checking all the cutting positions after the automatic landmark identification step. Although we did not find any inconsistency in this work, we consider that it is a recommended step when applying our pipeline for new analyses.

Visualization of the differences between groups. Here we mainly applied a nonparametric, multivariate permutation testing on Hotelling's T^2 statistics. Compared with the conventional Jacobian determinant (Qiu and Miller, 2008; Qiu et al., 2008; Qiu et al., 2009a; Qiu et al., 2010), the logarithmic transforms are applied to convert the tensors into vectors that are more tractable for Euclidean operations. On the other hand, standard multivariate random field theory may also be applicable to analyze the new multivariate statistics. For instance, in (Worsley et al., 2004; Taylor and Worsley, 2008), results based on random field theory for Roy's maximum root was proposed. The inference for Roy's maximum root is based on the Roy's union-intersection principle (Roy, 1953). Recently, Chung et al. (2010) used this statistic to quantify abnormal local shape variations of the amygdala in 22 high-functioning autistic subjects. Here since we used Hotelling T^2 test, the significant map results are like 2-sided tests and do not carry the direction information. To visualize the deformation directions, we defined a new measurement (Wang et al., 2011a) at each vertex k as

$$R^k = \frac{\sum_i^{N_1} \det J_{1i}^k}{\sum_j^{N_2} \det J_{2j}^k} \frac{N_2}{N_1} \tag{12}$$

where J_{1i}^k and J_{2j}^k are the Jacobian matrices for the ith subject in one group and the jth subject in another group, respectively, and N_1 and N_2 are the number of subjects in one group and in another group. The determinant of Jacobian matrix indicates the difference in size of the region in the individual subject compared to the template. When registering the two groups of subjects to a common template, R^k with values greater than 1 indicating that the surface area at that vertex is larger in one group when compared to the other group and vice versa for values smaller than 1. From **Fig. 15** we can see that, when comparing AD patients with healthy controls or MCI subjects

many challenges, such as different resolutions, high dimension, etc. How to combine the contextual information, e.g. considering the neighboring image information in the analysis, to improve statistical power still needs further investigation. We noticed some recent work (Du et al., 2011) has proposed new methods which integrate information of curves, surface and volumetric images. It could be a potential future work to improve hippocampal subfield analysis research.

Our algorithm is generic and may be useful for other subcortical structure analysis. There are two main caveats when applying the developed surface fluid registration method to study general subcortical surface registration problem. First, in the topology optimization step, the current algorithm requires two landmark cuts, which may restrict the applicability of the proposed method with other subcortical structures. Thus far, we have applied this algorithm to study putamen morphometry in prematurity study (Shi et al., 2012) and applied another similar algorithm (constrained harmonic map through flattening 3D surfaces (Wang et al., 2011b)) to study morphometry of thalamus (Wang et al., 2011a) and corpus collosum (Wang et al., 2012a) on prematurity and achieved some limited success. Since the subcortical structures are normalized in a common stereotaxic coordinate system in a controlled manner, we assume some geometry extreme positions can serve as geometrically valid and consistent landmarks across subjects in these work. However, it deserves more careful validation on whether these landmarks are also biologically valid and one should be cautious about how consistent they are for a population based study. Second, to map a hippocampal surface to a 2D plane, we introduce a few cuts on the surfaces. Currently, by introducing the same length cuts on consistent surfaces, we try to make sure that the induced boundaries are consistent across surfaces on the parameter domain and the flow computation is the same for vertices that are close to the boundaries as those in the internal areas. Although the cuts may not alter the geometry of the original surface, it could affect the quality of vertex correspondences near the two curves during the surface fluid registration. Even so, it is a logical conclusion from observing the maps in **Fig. 14** that the introduced boundaries do not seem to introduce artifacts and affect the statistical results. It shows the potential of our work for the proposed hippocampal surface morphometry analysis.

5. CONCLUSION

With conformal parameterization, we extended the inverse consistent image fluid registration method to match general surfaces. This has numerous applications in medical imaging. Our examples of matching various hippocampal surfaces are relevant for mapping how degenerative diseases affect the brain, as well as building statistical shape models to detect the anatomical effects of disease, aging, or development. The hippocampus is used as specific examples, but the method is general and is applicable in principle to cortical and other subcortical surfaces.

Our surface-based fluid registration system automates the matching of surfaces by computing a correspondence field guided by the differences of features between the surfaces. This is a natural idea, in that it uses conformal

parameterization to transform a surface matching problem into an image registration problem. Whether or not this approach provides a more relevant correspondences than those afforded by other criteria (mutual information, neural nets, or hand landmarking) requires careful validation for each application. Optimal correspondence depends more on utility for a particular application than on anatomical homology. Because different correspondence principles produce different shape models, we plan to compare them in future work for detecting group differences and genetic influence in brain structures.

As we described in Results section, the inverse consistent fluid flow that matches one surface to another was computed with the surface feature images and the images were computed by summing up local conformal factor and mean curvature and linearly scaling the dynamic range to [0, 255]. It is possible that some dynamic ranges in the features will be scaled into just one range in the image. Thus an improvement of the accuracy of the fluid registration is to compute the flow directly on the triangular surface coordinates with the original features and finite element method. We plan to pursue this direction in our future work.

As we discussed in the Results section, our results agree with some literature (Morra et al., 2009a; Pievani et al., 2011). Similar to other surface-based hippocampal subfield analysis work (Thompson et al., 2004a; Morra et al., 2009a; Qiu et al., 2009b; Apostolova et al., 2010a), our method is able to detect some specific significantly different regions. With our current statistical validation strategies, permutation test and false discovery rate, our results match with results from two other methods, SPHARM and FIRST. The spreading results, e.g. between controls and MCI/AD, do not indicate the differences are simply smoothed/averaged over the whole structure. Our future work will further investigate how to apply these detected statistical group differences with drug trials (Gutman et al., 2012), classification (Yuan et al., 2012), and progression (Ye et al., 2012).

In future, we will also apply our inverse consistent surface fluid registration framework to work with other surface features, such as surface heat kernel signature (Sun et al., 2009b), Beltrami coefficients (Lui et al., 2010), etc. The proposed multivariate measures may help in detection of degenerative effects, and may also benefit imaging genetics research (Ho et al., 2010). In this work, we used the group difference study as an application. With multivariate features, it is natural to apply machine learning methods to perform computer-assisted diagnosis and predict future clinical decline (Sun et al., 2009a; Kohannim et al., 2010; Wang et al., 2010a). Our future plan is to incorporate our system with some other machine learning tools, such as support vector machine (Vapnik, 1998), sparse learning (Candès and Tao, 2005), etc., and build a system which may identify imaging biomarkers that are able to evaluate AD related disease burden and predict progression and response to interventions. The combined system may offer a surface-based subcortical structure morphometry tool to detect the anatomical effects on ageing and disease.

APPENDIX A

With conformal parameterization, the Riemann metric is defined as:

$$[g_{ij}] = \begin{bmatrix} g_{11} & g_{12} \\ g_{21} & g_{22} \end{bmatrix} = \begin{bmatrix} \lambda & 0 \\ 0 & \lambda \end{bmatrix}$$

The inverse of $[g_{ij}]$ is:

$$[g^{ij}] = \begin{bmatrix} g^{11} & g^{12} \\ g^{21} & g^{22} \end{bmatrix} = \begin{bmatrix} 1/\lambda & 0 \\ 0 & 1/\lambda \end{bmatrix}$$

We now provide the expression in general coordinates of the differential operators that appear in **Eq. 9** (Aris, 1989; Stam, 2003).

Gradient:

$$\nabla_S \varphi = g^{ij} \frac{\partial \varphi}{\partial x_j} = g^{i1} \frac{\partial \varphi}{\partial x_1} + g^{i2} \frac{\partial \varphi}{\partial x_2} = \begin{bmatrix} g^{11} \frac{\partial \varphi}{\partial x_1} + g^{12} \frac{\partial \varphi}{\partial x_2} \\ g^{21} \frac{\partial \varphi}{\partial x_1} + g^{22} \frac{\partial \varphi}{\partial x_2} \end{bmatrix}$$

Thus the gradient operator ∇_S can be written as:

$$\nabla_S = \begin{bmatrix} g^{11} \frac{\partial}{\partial x_1} + g^{12} \frac{\partial}{\partial x_2} \\ g^{21} \frac{\partial}{\partial x_1} + g^{22} \frac{\partial}{\partial x_2} \end{bmatrix}$$

Divergence:

$$\nabla_S \cdot u = \frac{1}{\sqrt{g}} \frac{\partial}{\partial x_i} \left(\sqrt{g} u_i\right) = \frac{1}{\sqrt{g}} \left(\frac{\partial}{\partial x_1} \left(\sqrt{g} u_1\right) + \frac{\partial}{\partial x_2} \left(\sqrt{g} u_2\right)\right)$$

where $u = \begin{bmatrix} u_1 \\ u_2 \end{bmatrix}$ and $\sqrt{g} = \sqrt{\det\left([g_{ij}]\right)} = \sqrt{g_{11} g_{22} - g_{12} g_{21}}$.

The Laplacian can be computed by gradient and divergence as:

$$\Delta_S \varphi = \nabla_S \cdot (\nabla_S \varphi) = \frac{1}{\sqrt{g}} \left(\frac{\partial}{\partial x_1} \left(\sqrt{g} g^{11} \frac{\partial \varphi}{\partial x_1} + \sqrt{g} g^{12} \frac{\partial \varphi}{\partial x_2}\right) + \frac{\partial}{\partial x_2} \left(\sqrt{g} g^{21} \frac{\partial \varphi}{\partial x_1} + \sqrt{g} g^{22} \frac{\partial \varphi}{\partial x_2}\right)\right)$$

Given conformal parameterization $\phi: S \to \mathbb{R}^2$, where $\sqrt{g} = \lambda, g^{11} = g^{22} = \frac{1}{\lambda}, g^{12} = g^{21} = 0$, we have

$$\Delta_S v = \frac{1}{\lambda} \Delta v$$

For a velocity field $v = \begin{bmatrix} v_1 \\ v_2 \end{bmatrix}$, $\nabla_S (\nabla_S \cdot v) = \nabla \left(g^{11} \frac{\partial v_1}{\partial x_1} + g^{12} \frac{\partial v_1}{\partial x_2} + g^{21} \frac{\partial v_2}{\partial x_1} + g^{22} \frac{\partial v_2}{\partial x_2}\right) = \frac{1}{\lambda} \nabla (\nabla \cdot v)$.

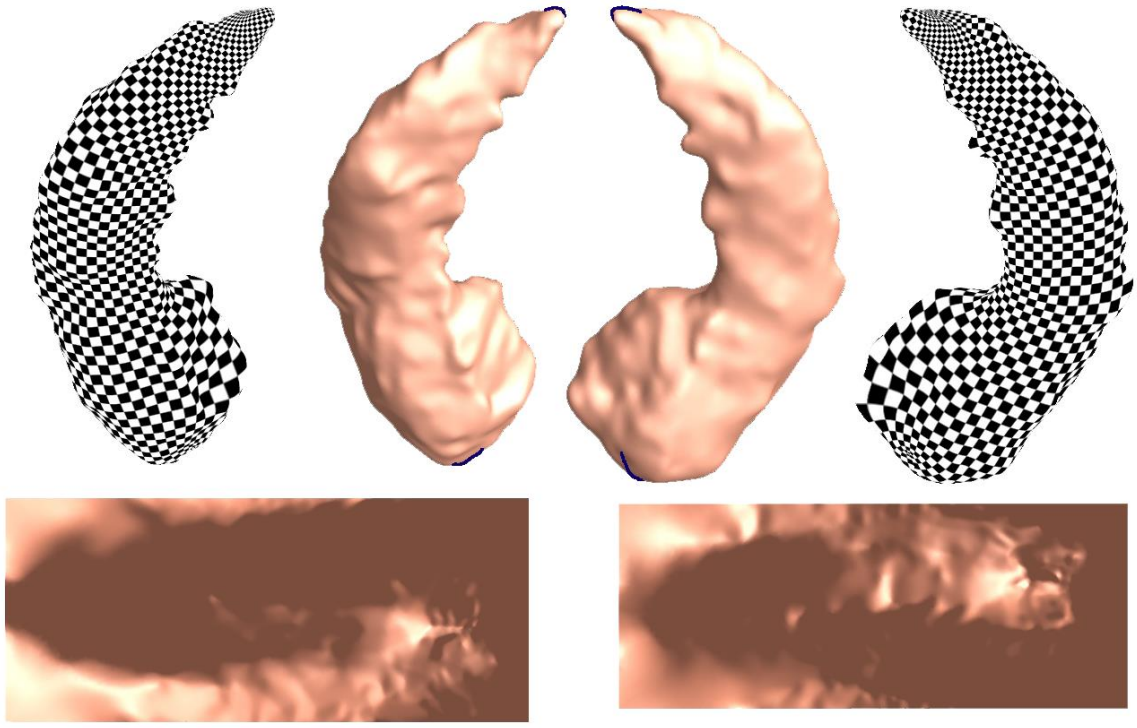

(a) Conformal Parameterization of Hippocampus with Holomorphic 1-Forms

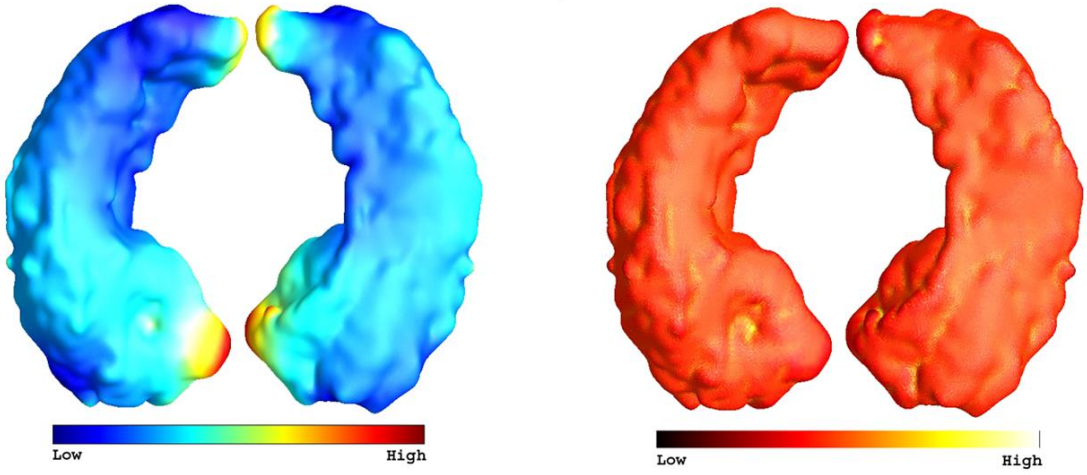

(b) Conformal Factor and Mean Curvature

Figure 3. Illustration of surface conformal parameterization (a) and geometric features (b). In (a), the boundaries generated in the topology optimization step were labeled in blue color. Each side of the hippocampal surface was conformally mapped to a rectangle in the parameter domain. The overlaid checkboard texture is used to demonstrate angle preserving property; the shading effect on the parameter space was generated by rendering the original 3D surface with the surface normal directions on each point. In (b), surface geometric features were color coded. The parameterization results and geometric features were used for surface registration and morphometric analysis.

Figure 6. Illustration of inverse consistent surface fluid registration on map of local shape differences (p-values) between different diagnostic groups, based on the mutivariate TBM method with hippocampal surfaces from ADNI baseline dataset, which were automatically segmented by FIRST. (a), (b), (c) are group difference p-maps between AD and control, AD and MCI, MCI and control, respectively, in 194 AD, 402 MCI, and 228 control subjects. The p-map color scale is the same as Fig. 8. (d), (e), (f) are the CDF plots.

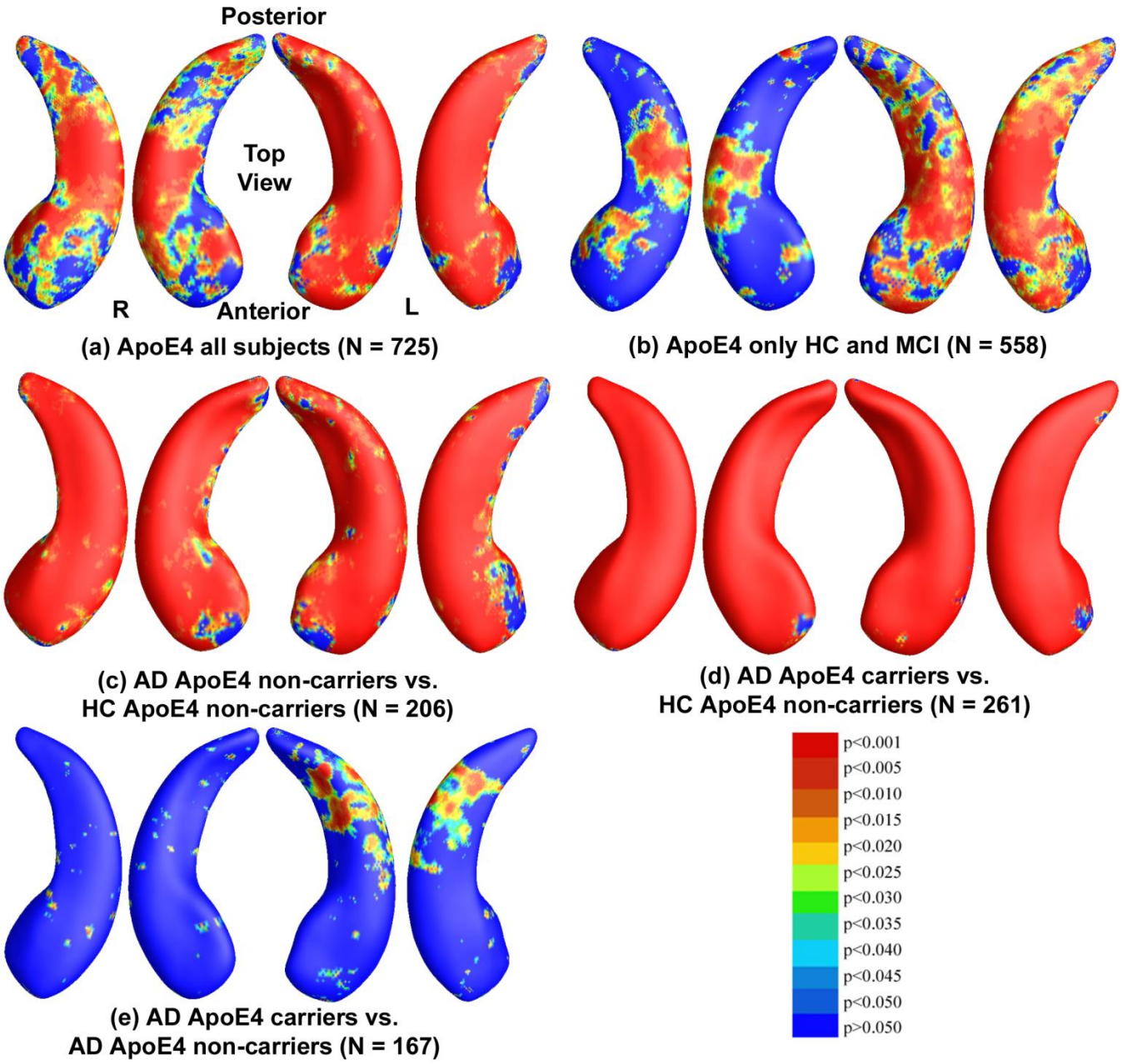

Figure 8. Significance maps for ApoE4 effects with inverse consistent surface fluid registration.

Figure 11. Cumulative distribution function plots comparison for ApoE4 effects with mTBM as the surface morphometry statistics.

Figure 13. Comparison of the inverse consistent surface fluid registration with and without the area distortion correction term in **Eq. 5**. We visualize the pull-back metric by drawing those equal-spaced black strips defined on the target surfaces back to the source surfaces. Overall the registration results with the area distortion correction ((c) and (d)) are more uniform, i.e. less drastic area distortion strips, than the ones without the area distortion correction ((e) and (f)).

REFERENCE

Agosta, F., Vossel, K.A., Miller, B.L., Migliaccio, R., Bonasera, S.J., Filippi, M., Boxer, A.L., Karydas, A., Possin, K.L., Gorno-Tempini, M.L., 2009. Apolipoprotein E epsilon4 is associated with disease-specific effects on brain atrophy in Alzheimer's disease and frontotemporal dementia. Proc Natl Acad Sci U S A 106(6), 2018-2022.

Alhadidi, A., Cevidanes, L.H., Paniagua, B., Cook, R., Festy, F., Tyndall, D., 2012. 3D quantification of mandibular asymmetry using the SPHARM-PDM tool box. Int J Comput Assist Radiol Surg 7(2), 265-271.

Apostolova, L.G., Morra, J.H., Green, A.E., Hwang, K.S., Avedissian, C., Woo, E., Cummings, J.L., Toga, A.W., Jack, C.R., Jr., Weiner, M.W., Thompson, P.M., 2010a. Automated 3D mapping of baseline and 12-month associations between three verbal memory measures and hippocampal atrophy in 490 ADNI subjects. Neuroimage 51(1), 488-499.

Apostolova, L.G., Mosconi, L., Thompson, P.M., Green, A.E., Hwang, K.S., Ramirez, A., Mistur, R., Tsui, W.H., de Leon, M.J., 2010b. Subregional hippocampal atrophy predicts Alzheimer's dementia in the cognitively normal. Neurobiol Aging 31(7), 1077-1088.

Apostolova, L.G., Thompson, P.M., Green, A.E., Hwang, K.S., Zoumalan, C., Jack, C.R., Jr., Harvey, D.J., Petersen, R.C., Thal, L.J., Aisen, P.S., Toga, A.W., Cummings, J.L., Decarli, C.S., 2010c. 3D comparison of low, intermediate, and advanced hippocampal atrophy in MCI. Hum Brain Mapp 31(5), 786-797.

Aris, R., 1989. Vectors, Tensors and the Basic Equations of Fluid Mechanics. Dover, New York.

Arsigny, V., Fillard, P., Pennec, X., Ayache, N., 2006. Log-Euclidean Metrics for Fast and Simple Calculus on Diffusion Tensors. Magn. Reson. Med. 56(2), 411-421.

Ashburner, J., Hutton, C., Frackowiak, R., Johnsrude, I., Price, C., Friston, K., 1998. Identifying global anatomical differences: deformation-based morphometry. Human Brain Mapping 6(5-6), 348-357.

Auzias, G., Colliot, O., Glaunes, J.A., Perrot, M., Mangin, J.F., Trouve, A., Baillet, S., 2011. Diffeomorphic brain registration under exhaustive sulcal constraints. IEEE Trans Med Imaging 30(6), 1214-1227.

Bajaj, C.L., Xu, G., 2003. Anisotropic diffusion of surfaces and functions on surfaces. ACM Transactions on Graphics 22(1), 4-32.

Bakircioglu, M., Joshi, S., Miller, M.I., 1999. Landmark Matching on Brain Surfaces via Large Deformation Diffeomorphisms on the Sphere. Proc. SPIE Medical Imaging, pp. 710-715.

Balasubramanian, M., Polimeni, J.R., Schwartz, E.L., 2010. Near-isometric flattening of brain surfaces. Neuroimage 51(2), 694-703.

Benjamini, Y., Hochberg, Y., 1995. Controlling the False Discovery Rate: A Practical and Powerful Approach to Multiple Testing. Journal of the Royal Statistical Society. Series B (Methodological) 57(1), 289-300.

Bennett, D.A., De Jager, P.L., Leurgans, S.E., Schneider, J.A., 2009. Neuropathologic intermediate phenotypes enhance association to Alzheimer susceptibility alleles. Neurology 72(17), 1495-1503.

Berg, L., 1988. Clinical Dementia Rating (CDR). Psychopharmacol Bull 24(4), 637-639.

Blacker, D., Haines, J.L., Rodes, L., Terwedow, H., Go, R.C., Harrell, L.E., Perry, R.T., Bassett, S.S., Chase, G., Meyers, D., Albert, M.S., Tanzi, R., 1997. ApoE-4 and age at onset of Alzheimer's disease: the NIMH genetics initiative. Neurology 48(1), 139-147.

Bossa, M., Zacur, E., Olmos, S., 2011. Statistical analysis of relative pose information of subcortical nuclei: application on ADNI data. Neuroimage 55(3), 999-1008.

Boyer, D.M., Lipman, Y., St Clair, E., Puente, J., Patel, B.A., Funkhouser, T., Jernvall, J., Daubechies, I., 2011. Algorithms to automatically quantify the geometric similarity of anatomical surfaces. Proc Natl Acad Sci U S A 108(45), 18221-18226.

Bro-Nielsen, M., Gramkow, C., 1996. Fast fluid registration of medical images. Visualization in Biomedical Computing (VBC'96). . Springer, pp. 267-276.

Brodmann, K., 1909. Vergleichende Lokalisationslehre der Grosshirnrinde in ihren Prinzipien dargestellt auf Grund des Zellenbaues. Johann Ambrosius Barth Verlag.

Bronstein, A.M., Bronstein, M.M., Kimmel, R., 2006. Generalized multidimensional scaling: a framework for isometry-invariant partial surface matching. Proc Natl Acad Sci U S A 103(5), 1168-1172.

Candès, E.J., Tao, T., 2005. Decoding by linear programming. Information Theory, IEEE Transactions on 51(12), 4203-4215.

Cao, J., Worsley, K.J., 1999. The detection of local shape changes via the geometry of Hotelling's T^2 fields. Ann. Statist 27(3), 925-942.

Cardenas, V.A., Chao, L.L., Studholme, C., Yaffe, K., Miller, B.L., Madison, C., Buckley, S.T., Mungas, D., Schuff, N., Weiner, M.W., 2011. Brain atrophy associated with baseline and longitudinal measures of cognition. Neurobiol Aging 32(4), 572-580.

Carmichael, D., 2011. Hippocampal Volume and Morphometry in a Cognitively Impaired Population at Increased Risk of Schizophrenia: The Edinburgh Study of Comorbidity. The University of Edinburgh.

Caselli, R.J., Walker, D., Sue, L., Sabbagh, M., Beach, T., 2010. Amyloid load in nondemented brains correlates with APOE e4. Neurosci Lett 473(3), 168-171.

Geroldi, C., Pihlajamaki, M., Laakso, M.P., DeCarli, C., Beltramello, A., Bianchetti, A., Soininen, H., Trabucchi, M., Frisoni, G.B., 1999. APOE-epsilon4 is associated with less frontal and more medial temporal lobe atrophy in AD. Neurology 53(8), 1825-1832.

Goebel, R., 2012. BrainVoyager--past, present, future. Neuroimage 62(2), 748-756.

Gouras, G.K., Relkin, N.R., Sweeney, D., Munoz, D.G., Mackenzie, I.R., Gandy, S., 1997. Increased apolipoprotein E epsilon 4 in epilepsy with senile plaques. Ann Neurol 41(3), 402-404.

Gu, X., Vemuri, B., 2004. Matching 3D shapes using 2D conformal representations. Med Image Comput Comput Assist Interv. Springer, pp. 771-780.

Gu, X., Wang, Y., Chan, T.F., Thompson, P.M., Yau, S.-T., 2004a. Genus zero surface conformal mapping and its application to brain surface mapping. IEEE Trans. Med. Imag. 23(8), 949-958.

Gu, X., Wang, Y., Yau, S.-T., 2004b. Geometric Compression using Riemann Surface Structure. Communications in Information and Systems 3(3), 171-182.

Guggenheimer, H.W., 1977. Differential Geometry. Dover Publications.

Gutman, B.A., Hua, X., Rajagopalan, P., Chou, Y.-Y., Wang, Y., Yanovsky, I., Toga, A.W., Jack, C.R., Jr., Weiner, M.W., Thompson, P.M., 2012. Maximizing Power to Track Alzheimer's Disease and MCI Progression by LDA-Based Weighting of Longitudinal Ventricular Surface Features. Submitted to NeuroImage.

Han, X., Xu, C., Prince, J.L., 2003. A topology preserving level set method for geometric deformable models. Pattern Analysis and Machine Intelligence, IEEE Transactions on 25(6), 755-768.

Hasboun, D., Chantome, M., Zouaoui, A., Sahel, M., Deladoeuille, M., Sourour, N., Duyme, M., Baulac, M., Marsault, C., Dormont, D., 1996. MR determination of hippocampal volume: comparison of three methods. AJNR Am J Neuroradiol 17(6), 1091-1098.

Hashimoto, M., Yasuda, M., Tanimukai, S., Matsui, M., Hirono, N., Kazui, H., Mori, E., 2001. Apolipoprotein E epsilon 4 and the pattern of regional brain atrophy in Alzheimer's disease. Neurology 57(8), 1461-1466.

Hermosillo, G., 2002. Variational methods for multimodal image matching. Universit$\acutee$ de Nice (INRIA-ROBOTVIS), Sophia Antipolis, France.

Hickie, I., Naismith, S., Ward, P.B., Turner, K., Scott, E., Mitchell, P., Wilhelm, K., Parker, G., 2005. Reduced hippocampal volumes and memory loss in patients with early- and late-onset depression. Br J Psychiatry 186, 197-202.

Ho, A.J., Stein, J.L., Hua, X., Lee, S., Hibar, D.P., Leow, A.D., Dinov, I.D., Toga, A.W., Saykin, A.J., Shen, L., Foroud, T., Pankratz, N., Huentelman, M.J., Craig, D.W., Gerber, J.D., Allen, A.N., Corneveaux, J.J., Stephan, D.A., DeCarli, C.S., DeChairo, B.M., Potkin, S.G., Jack, C.R., Jr., Weiner, M.W., Raji, C.A., Lopez, O.L., Becker, J.T., Carmichael, O.T., Thompson, P.M., 2010.

A commonly carried allele of the obesity-related FTO gene is associated with reduced brain volume in the healthy elderly. Proc Natl Acad Sci U S A 107(18), 8404-8409.

Holland, D., Brewer, J.B., Hagler, D.J., Fenema-Notestine, C., Dale, A.M., 2009. Subregional neuroanatomical change as a biomarker for Alzheimer's disease. Proc Natl Acad Sci U S A 106(49), 20954-20959.

Hoppe, H., 1996. Progressive meshes. Proceedings of the 23rd annual conference on Computer graphics and interactive techniques. ACM, pp. 99-108.

Hotelling, H., 1931. The generalization of Student's ratio. Ann. Math. Statist. 2, 360-378.

Hsiung, C.-C., 1997. A First Course in Differential Geometry. International Press.

Hua, X., Gutman, B., Boyle, C., Rajagopalan, P., Leow, A.D., Yanovsky, I., Kumar, A.R., Toga, A.W., Jack, C.R., Jr., Schuff, N., Alexander, G.E., Chen, K., Reiman, E.M., Weiner, M.W., Thompson, P.M., 2011. Accurate measurement of brain changes in longitudinal MRI scans using tensor-based morphometry. Neuroimage 57(1), 5-14.

Jack, C.R., Jr., Slomkowski, M., Gracon, S., Hoover, T.M., Felmlee, J.P., Stewart, K., Xu, Y., Shiung, M., O'Brien, P.C., Cha, R., Knopman, D., Petersen, R.C., 2003. MRI as a biomarker of disease progression in a therapeutic trial of milameline for AD. Neurology 60(2), 253-260.

Jack, C.R., Jr., Shiung, M.M., Gunter, J.L., O'Brien, P.C., Weigand, S.D., Knopman, D.S., Boeve, B.F., Ivnik, R.J., Smith, G.E., Cha, R.H., Tangalos, E.G., Petersen, R.C., 2004. Comparison of different MRI brain atrophy rate measures with clinical disease progression in AD. Neurology 62(4), 591-600.

Jones, T.R., Durand, F., Desbrun, M., 2003. Non-iterative, feature-preserving mesh smoothing. ACM Transactions on Graphics 22(3), 943-949.

Kim, B., Boes, J.L., Frey, K.A., Meyer, C.R., 1997. Mutual information for automated unwarping of rat brain autoradiographs. NeuroImage 5(1), 31-40.

Kim, W.H., Pachauri, D., Hatt, C., Chung, M.K., Johnson, S.C., Singh, V., 2012. Wavelet based multi-scale shape features on arbitrary surfaces for cortical thickness discrimination Advances in Neural Information Processing Systems (NIPS), 1250-1258.

Kohannim, O., Hua, X., Hibar, D.P., Lee, S., Chou, Y.Y., Toga, A.W., Jack, C.R., Jr., Weiner, M.W., Thompson, P.M., 2010. Boosting power for clinical trials using classifiers based on multiple biomarkers. Neurobiol Aging 31(8), 1429-1442.

Kok, E., Haikonen, S., Luoto, T., Huhtala, H., Goebeler, S., Haapasalo, H., Karhunen, P.J., 2009. Apolipoprotein E-dependent accumulation of Alzheimer disease-related lesions begins in middle age. Ann Neurol 65(6), 650-657.

Reiman, E.M., Chen, K., Alexander, G.E., Caselli, R.J., Bandy, D., Osborne, D., Saunders, A.M., Hardy, J., 2005. Correlations between apolipoprotein E epsilon4 gene dose and brain-imaging measurements of regional hypometabolism. Proc Natl Acad Sci U S A 102(23), 8299-8302.

Reiman, E.M., Chen, K., Liu, X., Bandy, D., Yu, M., Lee, W., Ayutyanont, N., Keppler, J., Reeder, S.A., Langbaum, J.B., Alexander, G.E., Klunk, W.E., Mathis, C.A., Price, J.C., Aizenstein, H.J., DeKosky, S.T., Caselli, R.J., 2009. Fibrillar amyloid-beta burden in cognitively normal people at 3 levels of genetic risk for Alzheimer's disease. Proc Natl Acad Sci U S A 106(16), 6820-6825.

Reuter, M., Rosas, H.D., Fischl, B., 2010. Highly accurate inverse consistent registration: a robust approach. Neuroimage 53(4), 1181-1196.

Reuter, M., Fischl, B., 2011. Avoiding asymmetry-induced bias in longitudinal image processing. Neuroimage 57(1), 19-21.

Rey, D., Subsol, G., Delingette, H., Ayache, N., 2002. Automatic detection and segmentation of evolving processes in 3D medical images: Application to multiple sclerosis. Med Image Anal 6(2), 163-179.

Ridha, B.H., Anderson, V.M., Barnes, J., Boyes, R.G., Price, S.L., Rossor, M.N., Whitwell, J.L., Jenkins, L., Black, R.S., Grundman, M., Fox, N.C., 2008. Volumetric MRI and cognitive measures in Alzheimer disease : comparison of markers of progression. J Neurol 255(4), 567-574.

Roy, S.N., 1953. On a Heuristic Method of Test Construction and its use in Multivariate Analysis. The Annals of Mathematical Statistics 24(2), 220-238.

Rueckert, D., Sonoda, L.I., Hayes, C., Hill, D.L., Leach, M.O., Hawkes, D.J., 1999. Nonrigid registration using free-form deformations: application to breast MR images. IEEE Trans Med Imaging 18(8), 712-721.

Sander, P.V., Snyder, J., Gortler, S.J., Hoppe, H., 2001. Texture mapping progressive meshes. Proceedings of the 28th annual conference on Computer graphics and interactive techniques. ACM, pp. 409-416.

Schreiner, J., Asirvatham, A., Praun, E., Hoppe, H., 2004. Inter-surface mapping. ACM SIGGRAPH 2004 Papers. ACM, Los Angeles, California, pp. 870-877.

Schwartz, E.L., Shaw, A., Wolfson, E., 1989. A Numerical Solution to the Generalized Mapmaker's Problem: Flattening Nonconvex Polyhedral Surfaces. IEEE Trans. Patt. Anal. Mach. Intell. 11(9), 1005-1008.

Shattuck, D.W., Leahy, R.M., 2002. BrainSuite: an automated cortical surface identification tool. Med Image Anal 6(2), 129-142.

Shen, D., Davatzikos, C., 2002. HAMMER: hierarchical attribute matching mechanism for elastic registration. IEEE Trans Med Imaging 21(11), 1421-1439.

Shen, L., Makedon, F., 2006. Spherical mapping for processing of 3D closed surfaces. Image and Vision Computing 24(7), 743-761.

Shepard, R., 1962. The analysis of proximities: Multidimensional scaling with an unknown distance function. II. Psychometrika 27(3), 219-246.

Shi, J., Wang, Y., Ceschin, R., An, X., Nelson, M.D., Panigrahy, A., Leporé, N., 2012. Surface Fluid Registration and Multivariate Tensor-based Morphometry in NewBorns – the Effects of Prematurity on the Putamen. Asia-Pacific Signal and Information Processing Association Annual Summit and Conference (APSIPA ASC), Hollywood, CA, USA.

Shi, Y., Morra, J.H., Thompson, P.M., Toga, A.W., 2009. Inverse-Consistent Surface Mapping with Laplace-Beltrami Eigen-Features. Information Processing in Medical Imaging, 467-478.

Stam, J., 2003. Flows on surfaces of arbitrary topology. ACM Transactions on Graphics, pp. 724-731.

Stonnington, C.M., Chu, C., Kloppel, S., Jack, C.R., Jr., Ashburner, J., Frackowiak, R.S., 2010. Predicting clinical scores from magnetic resonance scans in Alzheimer's disease. Neuroimage 51(4), 1405-1413.

Strittmatter, W.J., Saunders, A.M., Schmechel, D., Pericak-Vance, M., Enghild, J., Salvesen, G.S., Roses, A.D., 1993. Apolipoprotein E: high-avidity binding to beta-amyloid and increased frequency of type 4 allele in late-onset familial Alzheimer disease. Proc Natl Acad Sci U S A 90(5), 1977-1981.

Styner, M., Lieberman, J.A., McClure, R.K., Weinberger, D.R., Jones, D.W., Gerig, G., 2005. Morphometric analysis of lateral ventricles in schizophrenia and healthy controls regarding genetic and disease-specific factors. Proc. Natl. Acad. Sci. U. S. A. 102(13), 4872-4877.

Styner, M., Oguz, I., Xu, S., Brechbühler, C., Pantazis, D., Levitt, J.L., Shenton, M.E., Gerig, G., 2006. Framework for the Statistical Shape Analysis of Brain Structures using SPHARM-PDM. Insight Journal(1071), 242-250.

Sun, D., van Erp, T.G.M., Thompson, P.M., Bearden, C.E., Daley, M., Kushan, L., Hardt, M.E., Nuechterlein, K.H., Toga, A.W., Cannon, T.D., 2009a. Elucidating a Magnetic Resonance Imaging-Based Neuroanatomic Biomarker for Psychosis: Classification Analysis Using Probabilistic Brain Atlas and Machine Learning Algorithms. Biological Psychiatry 66(11), 1055-1060.

Sun, J., Ovsjanikov, M., Guibas, L., 2009b. A concise and provably informative multi-scale signature based on heat diffusion. Proceedings of the Symposium on Geometry Processing. Eurographics Association, Berlin, Germany, pp. 1383-1392.

Sun, X., Rosin, P.L., Martin, R.R., Langbein, F.C., 2007. Fast and Effective Feature-Preserving Mesh Denoising IEEE Transactions on Visualization and Computer Graphics 13(5), 925-938.

Winkler, A.M., Kochunov, P., Blangero, J., Almasy, L., Zilles, K., Fox, P.T., Duggirala, R., Glahn, D.C., 2010. Cortical thickness or grey matter volume? The importance of selecting the phenotype for imaging genetics studies. NeuroImage 53(3), 1135-1146.

Winkler, A.M., Sabuncu, M.R., Yeo, B.T., Fischl, B., Greve, D.N., Kochunov, P., Nichols, T.E., Blangero, J., Glahn, D.C., 2012. Measuring and comparing brain cortical surface area and other areal quantities. Neuroimage 61(4), 1428-1443.

Wolz, R., Heckemann, R.A., Aljabar, P., Hajnal, J.V., Hammers, A., Lötjönen, J., Rueckert, D., 2010. Measurement of hippocampal atrophy using 4D graph-cut segmentation: Application to ADNI. NeuroImage 52(1), 109-118.

Worsley, K.J., Taylor, J.E., Tomaiuolo, F., Lerch, J., 2004. Unified univariate and multivariate random field theory. Neuroimage 23 Suppl 1, S189-195.

Yanovsky, I., Leow, A.D., Lee, S., Osher, S.J., Thompson, P.M., 2009. Comparing registration methods for mapping brain change using tensor-based morphometry. Med Image Anal 13(5), 679-700.

Yassa, M.A., Stark, S.M., Bakker, A., Albert, M.S., Gallagher, M., Stark, C.E., 2010. High-resolution structural and functional MRI of hippocampal CA3 and dentate gyrus in patients with amnestic Mild Cognitive Impairment. Neuroimage 51(3), 1242-1252.

Ye, J., Farnum, M., Yang, E., Verbeeck, R., Lobanov, V., Raghavan, N., Novak, G., Dibernardo, A., Narayan, V.A., 2012. Sparse learning and stability selection for predicting MCI to AD conversion using baseline ADNI data. BMC Neurol 12(1), 46.

Yeo, B.T., Sabuncu, M.R., Vercauteren, T., Ayache, N., Fischl, B., Golland, P., 2010. Spherical demons: fast diffeomorphic landmark-free surface registration. IEEE Trans Med Imaging 29(3), 650-668.

Ystad, M.A., Lundervold, A.J., Wehling, E., Espeseth, T., Rootwelt, H., Westlye, L.T., Andersson, M., Adolfsdottir, S., Geitung, J.T., Fjell, A.M., Reinvang, I., Lundervold, A., 2009. Hippocampal volumes are important predictors for memory function in elderly women. BMC Med Imaging 9, 17.

Yuan, L., Wang, Y., Thompson, P.M., Narayan, V.A., Ye, J., 2012. Multi-source feature learning for joint analysis of incomplete multiple heterogeneous neuroimaging data. Neuroimage 61(3), 622-632.

Yushkevich, P.A., Piven, J., Hazlett, H.C., Smith, R.G., Ho, S., Gee, J.C., Gerig, G., 2006a. User-guided 3D active contour segmentation of anatomical structures: significantly improved efficiency and reliability. Neuroimage 31(3), 1116-1128.

Yushkevich, P.A., Zhang, H., Gee, J.C., 2006b. Continuous medial representation for anatomical structures. IEEE Trans Med Imaging 25(12), 1547-1564.